Soft Tactile Sensor Arrays for Force Feedback in Micromanipulation

Frank L. Hammond III, *Member, IEEE*, Rebecca K. Kramer, Qian Wan, Robert D. Howe, *Fellow, IEEE*, and Robert J. Wood, *Member, IEEE*

***Abstract*— This paper describes the design, fabrication, and experimental validation of a soft tactile sensor array for submillimeter contact localization and contact force measurement in micromanipulation. The geometry and placement of conductive liquid microchannels embedded within the elastic sensor body are optimized to provide high sensitivity for representative micromanipulation tasks and to overcome functional limitations seen in previous soft tactile sensor research. Mechanical testing of the numerically optimized sensor prototype demonstrates sensitivity to normal contact forces of <50 mN and submillimeter contact localization resolution. Tactile sensing experiments demonstrate the ability to infer the abstract geometries and motions of objects imparting force on the sensor surface by analyzing microchannel deformation patterns.**

***Index Terms*— Haptic feedback, micromanipulation, numerical design optimization, force feedback, soft sensors, tactile sensing.**

I. Introduction

TACTILE sensing is considered by many to be a critical component in the advancement of medical procedures and manufacturing processes involving micromanipulation. Dexterous handling of small, delicate structures such as micromechanisms, surgical needles (Fig. 1), and soft, compliant biological tissues requires precise sensing and modulation of manipulation forces in order to prevent unintended damage. However, the micromanipulation methods used in surgery and manufacturing typically do not permit the force sensing and contact localization capabilities required to handle micro-scale objects without applying excessive forces - due in large part to the magnitude of tool-object interaction forces and the length of the instruments used [1]–[4].

In certain micromanipulation tasks it is possible to compensate for the absence of direct haptic feedback by the use of visual cues, such as the changes in material reflectance or shading on the surface of soft, deformable objects (biological tissues), to estimate applied forces [5], or by precisely structuring the workspace such that object locations and orientations are known (e.g. automated pick-and-place assembly tasks). In unstructured environments where visual acuity is poor, motion is highly constrained, and objects are too rigid to deform significantly under expected manipulation forces, the lack of haptic feedback can markedly reduce the speed and accuracy of manipulation and render conventional micromanipulation methods unsafe or intractable. This is especially true in microsurgical procedures, where excessive force application can easily damage surgical tools and lead to iatrogenic tissue trauma [6]–[8].

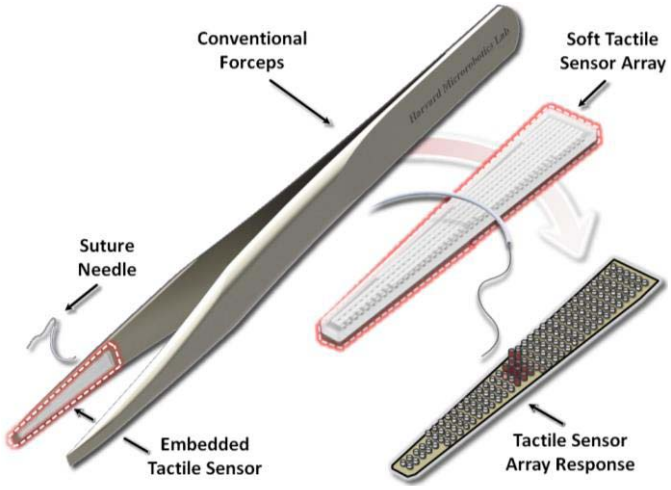

Fig. 1. Conceptual drawing of a soft tactile sensor array mounted on conventional forceps and responding to forces used to grasp a needle.

Several innovations have been made in recent years to facilitate haptic feedback in micromanipulation, including piezoresistive strain gauges [9]–[12] and optical Fiber Bragg Grating (FBG) sensors [13] for tool-tip force measurement in microsurgery devices, piezoelectric polyvinylidine-floride (PVDF) films [14] and MEMS-based capacitive sensor arrays [15], [16] for tactile sensing in robotic micromanipulation, and monolithic MEMS-based force-sensing manipulators [17], [18]. All of these innovations enable precise force measurement or contact localization suitable for micromanipulation, but several of them also entail problems with fabrication cost, mechanical robustness, signal fidelity and temporal hysteresis, packaging and assembly limitations, and a lack of functional versatility that make them unfit for general-purpose micromanipulation.

Manuscript received October 29, 2013; revised December 8, 2013; accepted December 14, 2013. Date of publication January 2, 2014; date of current version March 11, 2014. This work was supported in part by the Wyss Institute for Biologically Inspired Engineering and in part by the National Science Foundation. The work of F. L. Hammond III was supported by the National Academy of Sciences through the Ford Foundation Post-Doctoral Fellowship Award. The associate editor coordinating the review of this paper and approving it for publication was Prof. Ravinder S. Dahiya.

F. L. Hammond III, Q. Wan, R. D. Howe, and R. J. Wood are with the Harvard School of Engineering and Applied Sciences, Cambridge, MA 02138 USA (e-mail: fhammond@seas.harvard.edu; qwan@seas.harvard.edu; howe@seas.harvard.edu; rjwood@seas.harvard.edu).

R. K. Kramer is with the School of Mechanical Engineering, Purdue University, West Lafayette, IN 47907 USA (e-mail: rebeccakramer@purdue.edu).

Color versions of one or more of the figures in this paper are available online at http://ieeexplore.ieee.org.

Digital Object Identifier 10.1109/JSEN.2013.2297380

Advances in flexible electronics have enabled a new class of soft, elastic, skin-like sensors that promise to improve the feasibility and flexibility of force and tactile sensing in micromanipulation. New sensor technologies such as stretchable conductors [19], single-walled carbon nanotubes, and conductive particle and liquid microchannel embedded elastomers [20]–[22], and elastomer-coated capacitive MEMS sensors [23] are mechanically robust and innately reduce peak forces in micromanipulation due to their compliance [24]. These soft sensors improve manipulation by conforming to object surfaces to increase contact friction, allowing stable grasps with smaller applied forces, and by enabling palpation to determine object geometry, mechanical properties [25], and an object's position within a microgripper.

In a previous study [26], we designed and experimentally validated a soft, conductive liquid-embedded tactile sensor array for micromanipulation, leveraging previous work on fabrication methods for such sensors [27], [28]. The proposed sensor demonstrated sensitivity to forces as low as 50 mN and contact localization on the order of 500 microns (sensor channel spacing), but the microchannel geometries used in the design caused both significant sensitivity mismatches between sensor layers and a mechanical channel pinching phenomenon that limited functionality of the sensor under higher loads.

The goal of this study is improve the capabilities of soft tactile sensor arrays for micromanipulation through design optimization. We use finite element analysis (FEA) to predict the performance of tactile sensors under expected manipulation loads and iteratively modify the geometries of both the conductive liquid embedded channels and the interstitial and surface elastomer layers to create sensor layers with improved ranges of sensitivity. Through experimental testing, we demonstrate these improved sensitivity ranges, verify the ability to localize forces imparted on the sensor, and demonstrate the capacity to estimate the geometry and motion of impinging objects by analyzing the sensor output patterns.

II. Sensor Design

A. Microchannel-Embedded Soft Sensor Principle

Soft tactile sensor array design is based on the principle that the geometry of a conductive liquid microchannel embedded in an elastic body will change when that body is deformed by compression or stretching, changing its electrical resistance. Assuming that the cross-sectional area of a rectangular microchannel and the electrical properties of the conductive liquid are known, microchannel geometries can be designed such that their total range of electrical resistance spans the range of expected pressures or forces that deform them, thus providing adequate sensitivity for target tasks [26].

The degree of microchannel deformation under a given load and, by extension, the overall sensitivity of the sensor, is governed by microchannel geometry, elastomer material properties, and the position of the embedded channel within the elastomer. Recent work [22] derived an analytical approximation to model changes in microchannel cross-section with respect to these variables. However, this analytical solution is not appropriate for cases where microchannels are relatively large with respect to the dimensions of the elastomer. In the case of tactile arrays, the microchannels are close in proximity both to the elastomer surface and to each other for higher sensitivity and spatial resolution. In order to design tactile sensor arrays that are sensitive enough for micromanipulation and that adhere to fabrication rules, we must model the sensor, simulate its non-linear elastic mechanics, and optimize the sensor topology using finite element analysis (FEA).

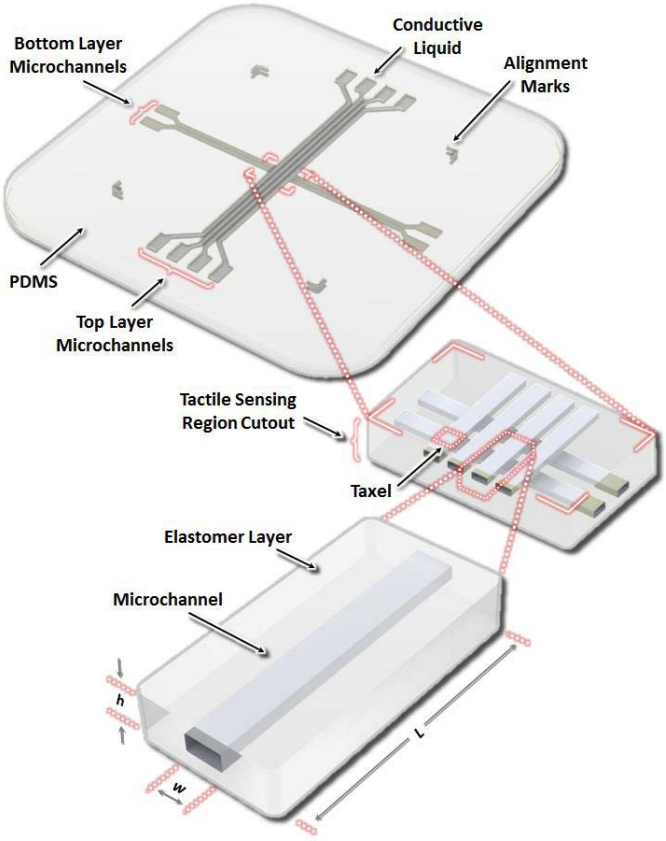

Fig. 2. Topology the soft tactile sensor test prototype with orthogonal microchannels for contact localization. A 'taxel' sensor region is highlighted, and major dimensions used to compute microchannel resistance are shown.

B. Tactile Sensor Topology

The proposed soft tactile sensor array is comprised of two layers of conductive liquid filled microchannels embedded in polydimethylsiloxane (PDMS) and arranged in an orthogonal configuration. One layer is used to localize contact in each direction in the sensor plane, creating a two-dimensional matrix of taxels (tactile pixels). These taxels can be used for contact localization and pressure measurement. The proposed sensor contains eight taxels in a 2x4 configuration (Fig. 2).

C. Target Application and Performance Requirements

The soft tactile sensor presented here is designed primarily for use in microsurgery and microassembly tasks. Performance requirements for this sensor are drawn from challenging clinical procedures including tissue resection in retinal microsurgery [11], [13] and small blood vessel and nerve anastomoses in cardiac surgery. These requirements are:

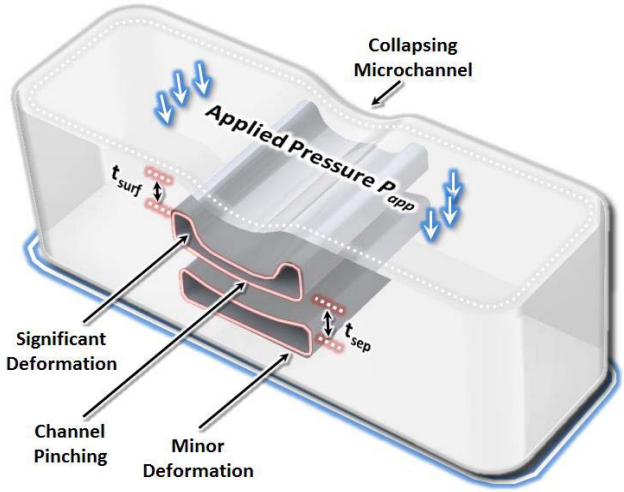

Fig. 3. Soft tactile sensor with the microchannel failures modes seen in [25]. The microchannels, shown here in parallel alignment for ease of illustration, exhibit behavior similar to channels aligned orthogonally.

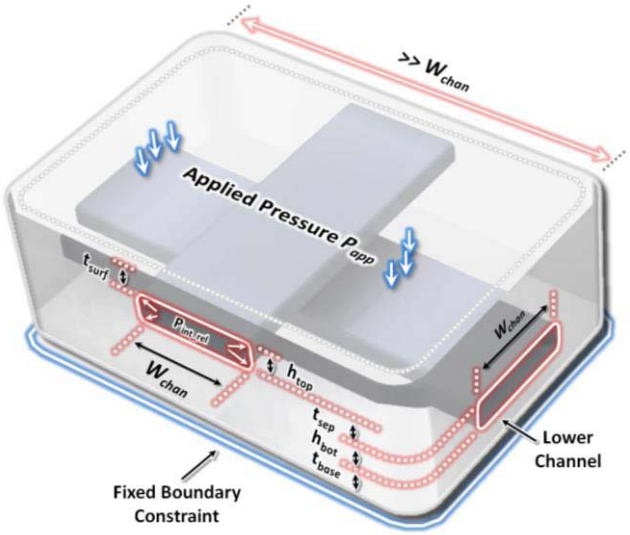

Fig. 4. Orthogonal microchannels in the top and bottom sensing layers and the parameters used for design optimization. Thickness of the material surrounding the channels is large enough that edge effects are negligible.

- *Force and Pressure Sensitivity:* Each individual sensor taxel must be sensitive to 25–250mN of force, assuming that microsurgical forces are no more than 1.0N [29] and are equally distributed over four taxels.
- *Spatial Resolution and Taxel Size:* The sensor must be no greater than 500μm in total thickness to fit on the functional surfaces of conventional microforceps tips.

In addition to quantitative requirements demanded by target applications, qualitative requirements have also been drawn from functional deficiencies seen in the previous tactile sensor design [26] (Fig. 3). These functional design requirements are:

- *Prevent Microchannel Pinching:* Microchannels remain patent under expected loads. If a microchannel collapses and the upper and lower walls adhere, its ability to sense over its full force range and localize contact is lost.
- *Matching Layer Sensitivity Ranges:* Microchannel layer sensitivity ranges must have significant overlap to support contact localization. Top-layer microchannels in previous designs saturated before bottom-layer microchannels exhibited any significant changes in resistance.

D. Sensor Design Optimization

The modeling, simulation, and optimization of the tactile sensor array microchannel geometry were done in COMSOL 4.3a Multiphysics software (COMSOL, Inc., Burlington, Massachusetts, USA). To capture the non-linear elastic behavior of the PDMS under large strain, the FEA simulation was set up as a stationary solid mechanics problem with a Mooney-Rivlin constitutive model. Other constitutive models such as Arruda-Boyce and neo-Hookean could also be used but for small strains (<25%) the model predictions are similar and the choice of model parameters is more important [30]. The PDMS material properties were set as follows: density $\rho = 965$ kg/m^3, Young's modulus $E = 500$kPa, Poisson's ratio $\nu = 0.485$, shear modulus $G = 250$kPa, and Mooney-Rivlin parameters $C_{10} = 75.5 \pm 2.7$kPa and $C_{01} = 5.7 \pm 3.7$kPa [31].

The soft tactile sensor model was given a fixed motion constraint on its bottom boundary to simulate attachment to a rigid tool surface and a uniform pressure field on its top boundary to simulate contact forces (Fig. 4). Another uniform pressure load which varied with changes in cross-sectional area was applied to the internal boundary of each microchannel. Pressure changes induced within the microchannel by the displacement of conductive liquid were roughly approximated using the expression shown in (1).

$$\Delta P_{int\_rel} = \eta \cdot P_{atm} \left(\frac{A_{init}}{A_{new}} - 1 \right) \tag{1}$$

Here, ΔP_{int_rel} is the relative internal pressure change of the microchannel assuming the external pressure is constant, A_{init} is the initial microchannel cross-sectional area, A_{new} is the cross-sectional area of the deformed microchannel, P_{atm} is the atmospheric pressure, and η is the expansion factor (set to 0.05) which accounts for the pressure relieved when a channel expands due to conductive liquid displacement. We assume that the entire channel has a new cross-sectional area A_{new} and the displaced liquid flows into a compliant reservoir which exerts pressure on the fluid, and which changes linearly with the displaced volume. The effect of conductive liquid viscosity, 1.99×10^{-3} Pa·s [32], on the response of the sensor was considered negligible as the operational range for target tactile sensor applications in microsurgery is only 2-3Hz [33].

The ranges and step sizes of all design variables used in the numerical optimization of the tactile sensor array are listed in Table I. These design variables include the heights of the top and bottom microchannels, h_{top} and h_{bot}, the thickness of the interstitial layer 'between top and bottom channel layers, t_{sep}, and the thickness of the sensor surface layer, t_{surf} (Fig. 4).

The thickness of the sensor substrate layer t_{base} is fixed at 100μm; thinner layers are difficult to handle manually during assembly. This layer also presumably lends little to sensor

TABLE I
SOFT TACTILE SENSOR DESIGN PARAMETERS

Parameter	*Min (μm)*	*Step(μm)*	*Max(μm)*
t_{surf}	50	10	150
h_{top}	20	20	60
t_{sep}	50	10	150
h_{bot}	20	20	60
t_{base}	Fixed at 100μm		
w_{chan}	Fixed at 200μm		

Fixed design parameters are set to the smallest values allowed by the current fabrication process.

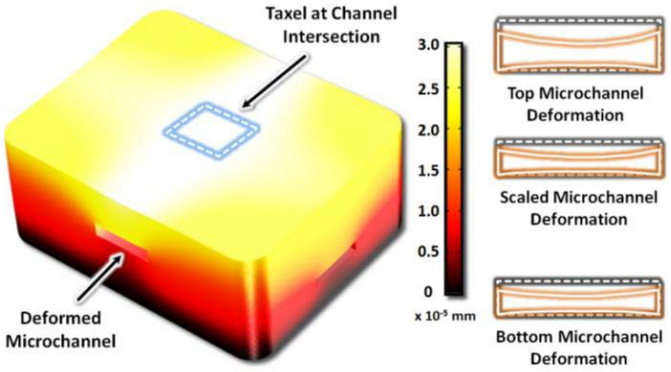

Fig. 5. A COMSOL rendering of optimized sensor geometry showing microchannel deformation under distributed load with deformed channel cross-sections (right). Relative resistance changes match to within 5%.

functionality and so it is minimized to decrease overall sensor height. The widths of microchannels w_{chan} and the septa between adjacent channels are fixed at 200μm because thinner channels exacerbate fabrication issues such as eGain injection resistance. Wider channels are feasible but would necessitate thinner channel septa (sensor width constraints), which have shown to delaminate from surrounding layers. As fabrication methods improve, smaller features will be possible.

Optimization of microchannel geometries was accomplished by exhaustively searching the design space and observing changes in deformation patterns as predicted by FEA. The objective measure for this optimization is a combination of the performance and functional requirements given in Section II.

- The separation between the top and bottom walls of the microchannels must not fall below 10% of initial channel height at any point during simulation (pinching).
- Sensitivity ranges of the microchannel layers must be such that the more sensitive layer does not collapse (top and bottom walls intersect) at the maximum applied pressure.
- Total sensor thickness t_{sensor} must be less than 500μm, with thinner designs preferred.

The design yielding the best matching sensitivity ranges, eliminating channel collapse problems, and having a height less than 500μm was deemed the optimal design solution. The quality function for each design is given by (2)

$$Q_{design} = \left(1 - \left|\frac{\Delta A_{top}}{A_{top}} - \frac{\Delta A_{bot}}{A_{bot}}\right|\right) \cdot \frac{t_{sensor_{\max}}}{t_{sensor}} \quad (2)$$

where Q_{design} is the quality metric, A_{bot} and A_{top} are cross-sectional areas of the bottom and top microchannels and ΔA_{bot} and ΔA_{top} are changes in these areas after sensor deformation. This formulation rewards topologies producing matching intra-layer sensitivity ranges and favors designs with low thickness.

COMSOL simulations of all sensor design variants were conducted by sweeping over the entire design parameter space. Each finite element model of the sensor was simulated using a coarse-element physics-controlled free tetrahedral mesh.

E. Optimization Results

Based upon the resulting data, the sensor design parameters with the highest tactile sensor design with the highest Q_{design} were $t_{surf} = 150\mu$m, $h_{top} = 60\mu$m, $t_{sep} = 80\mu$m, and $h_{bot} = 40\mu$m. These values produced a sensor 430μm in total thickness, with sensitivity ranges between layers that match to within 5% (Fig. 5), and able to measure the full range of expected micromanipulation forces without microchannel pinching.

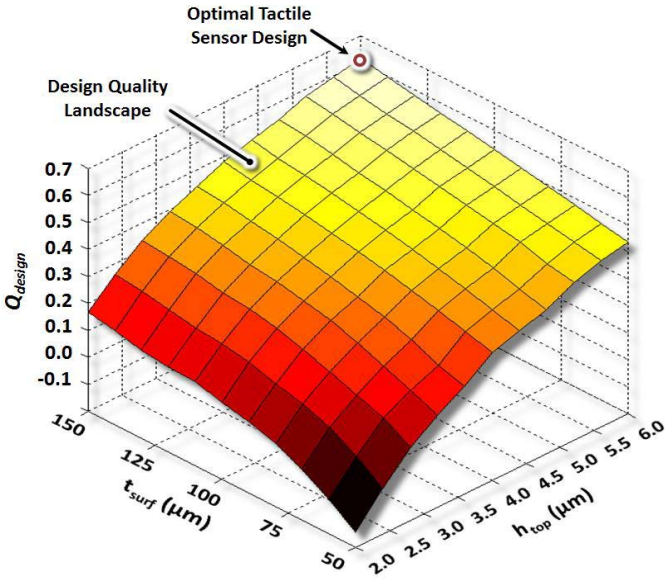

Fig. 6. A surface plot of sensor design quality versus sensor surface layer thickness t_{surf} and top microchannel height h_{top}.

Sensitivity analysis of Q_{design} variance over each of the design variables indicates that surface layer thickness t_{surf} and top microchannel height h_{top} have the greatest influence on Q_{design} (Fig. 6). Table II lists Q_{design} variance with respect to each design parameter. One qualitative explanation for the influence of t_{surf} and h_{top} is that surface layer thickness and top microchannel height determine how much energy is absorbed by the top layer before the bottom layer begins to deform and that, regardless of the bottom layer parameters, t_{sep} and h_{bot}, the top and bottom channels will exhibit significant

TABLE II
SENSITIVITY OF DESIGN QUALITY TO SENSOR DESIGN PARAMETERS

Parameter	*Range (μm)*	*min(Var(Q_i))*	*max(Var(Q_i))*	*μ(Var(Q_i))*
t_{surf}	100	0.0040	0.0341	0.0173
h_{top}	40	0.0015	0.1093	0.0462
t_{sep}	100	0.0000	0.0044	0.0009
h_{bot}	40	0.0002	0.0164	0.0069

Var(Q_i) is the set of variances of Q_{design} with respect to design parameter i for each unique combination of the remaining design parameters, set X. For parameter t_{surf}, *Var(Q_i)* is a set of 99 variances of Q_{design}. For parameter h_{top}, *Var(Q_i)* is a set of 363 variances (3).

differences in sensitivity if the top channels are too compliant.

$$Var(Q_i) = \left\{ Var(Q_i^1), Var(Q_i^2), \cdots, Var(Q_i^{W_i}) \right\}$$
$$W_i = \prod_{j=1}^{\#X} \#i \quad \forall j \neq i; \quad X = \left\{ t_{surf}, h_{top}, t_{sep}, h_{bot} \right\} \tag{3}$$

III. FABRICATION

A physical soft tactile sensor prototype was fabricated by means of a soft lithography process (see [27] for process illustration), using the optimization results above to inform the design. Photoresist (SU-8 2010) was spun onto clean silicon wafers to achieve the desired film thickness. After a soft-bake, the coated wafer was then patterned by use of a Kapton® polyimide photomask followed by a hard-bake and developer step. Silicon masters are used to mold three PDMS layers that result in the sensor array. A hydrophobic monolayer was introduced by vapor deposition to discourage adhesion between the silicon molds and subsequently cured PDMS. The wafers were placed in an evacuated chamber (20 mTorr) with an open vessel containing a few drops of Trichloro (1H, 1H, 2H, 2H-perfluorooctyl) silane (Aldrich) for 3 hours.

PDMS (Sylgard 184, Dow Corning, USA) was spin-coated in liquid form (10:1 weight ratio of elastomer base to curing agent) onto the silicon molds to result in thin elastomer films with known thickness. Each PDMS layer was cross-linked by heat-curing at 60 °C for 30-40 minutes. Layers were manually removed from the molds and bonded together with a thin layer of partially cured elastomer (spun at 3500 RPM for 30 seconds, then partially cured at 60 °C for 10 minutes). In order to accommodate subsequent filling of the channels within such a thin device using conventional syringe dispensing, small blocks ($\sim$1cm^2) of PDMS were adhered to each channel inlet and outlet location using uncured elastomer as adhesive glue. Introducing small holes into the adhered inlet and outlet blocks provided a convenient method for manual injection of the conductive liquid eutectic Gallium Indium (eGaIn, BASF). External wiring was achieved by manually cutting off the inlet/outlet block, inserting copper wire into the channel ends, and sealing the channels with a droplet of uncured PDMS. The resulting soft sensor array prototype is shown in Fig. 7.

EGaIn is amenable to the described fabrication method and has proven to be an effective sensing medium but is generally considered bioincompatible. It will be replaced in future designs by biocompatible liquid media.

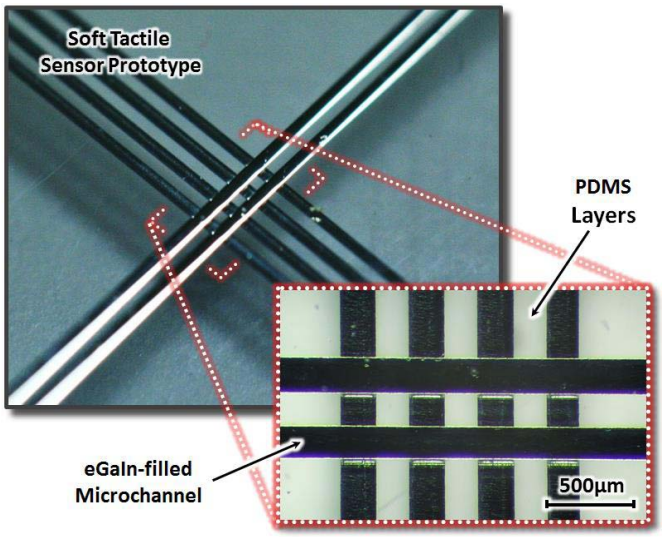

Fig. 7. The soft tactile sensor array prototype. Inset is a top-down view of the active sensing area. Channel resistance ranged between 1.3–1.5 Ohms.

IV. EXPERIMENTAL VALIDATION

The sensor validation experiment setup is comprised of data acquisition hardware and electromechanical testing equipment. The prototyped tactile sensor was empirically characterized by applying various forces to the sensor using a custom-designed sensor testbed and recording microchannel resistance changes.

A. Mechanical Testing Setup

The soft tactile sensor prototype was tested using an Instron 5540 Series electro-mechanical testing system (Instron Inc., USA) and custom designed soft tactile sensor testbed (Fig. 8). The Instron load frame was equipped with a 10N load cell capable of $\pm$0.5% reading accuracy down to 1/250 (40mN) of cell capacity. The custom designed tactile sensor testbed, rapid-prototyped using the Objet Connex500^{TM} 3D printer (Objet Inc., USA), consisted of a base plate for alignment of the tactile sensor, and clamp plate to hold the sensor in place in prevent wire pull-out, and circuit board for data acquisition, and a force application plate with interchangeable contact pads with sub-millimeter features (Fig. 9). Guide posts on the base plate help hold the force application plate in alignment with the sensor. Fig. 9 illustrates interaction between the contact pads and sensor array during experimental testing.

B. Data Acquisition

The eGaIn channels were wired to a 16-bit data acquisition board through a set of voltage divider circuits. Each microchannel was connected to a single divider with a reference resistor R_{ref} of 10Ω and a common power source V_S of 1.0V (Fig. 10). Increases in the electrical resistance R_{chan}

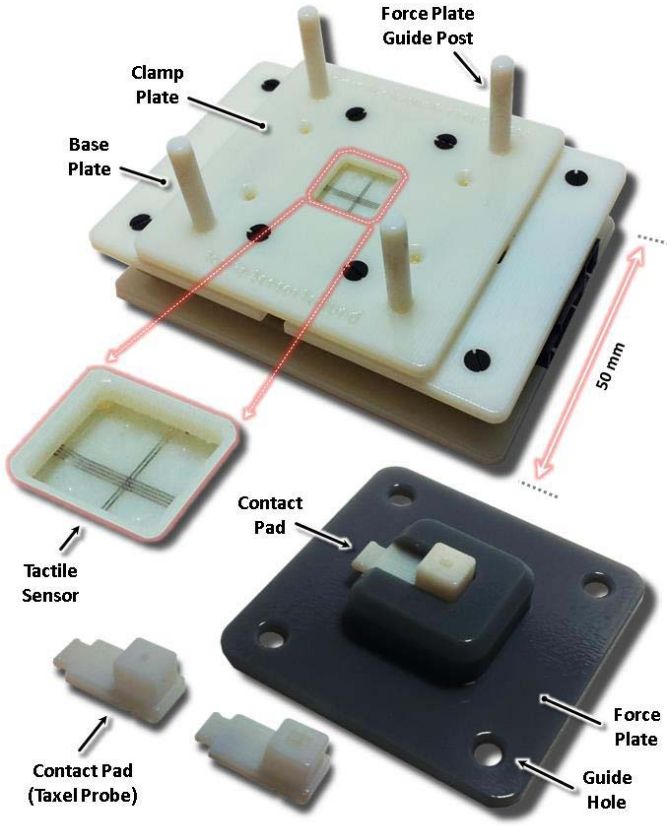

Fig. 8. Tactile sensor testbed with base plate and clamp plate used to secure the sensor (top) and force application plate to apply forces. The underside of the force application plate is shown (bottom) with removable contact pads.

of an eGaIn channel due to external forces cause a voltage increase at the divider output node (4).

$$V_{chan} = \frac{R_{chan}}{R_{ref} + R_{chan}} \cdot V_S \tag{4}$$

The analog voltage divider signals for each of the six microchannels were acquired at 1kHz. The voltages reported throughput this paper are voltages across the sensor channels.

C. Mechanical Test Procedure

The soft tactile sensor prototype was mounted to the sensor testbed base plate and mechanically tested using four different contact pads, shown in Fig. 9. For each contact pad, the Instron load frame applied normal force to the sensor by slowly compressing the sensor at a rate of 500μm/min until the maximum compressive load of 250mN was reached, after which the Instron load frame returned to the initial position. Data were also recorded for soft tactile sensor array response to dynamic loading. This loading was induced manually using a mechanical probe with a 2mm spherical tip which was rolled over the sensor surface at an average velocity of 470μm/s and with an average normal force of 780mN.

From these tests, three important sensor performance characteristics were analyzed:

- *Matching Microchannel Sensitivity Ranges:* Demonstrated by applying force over one taxel and measuring the response of both top and bottom microchannel.

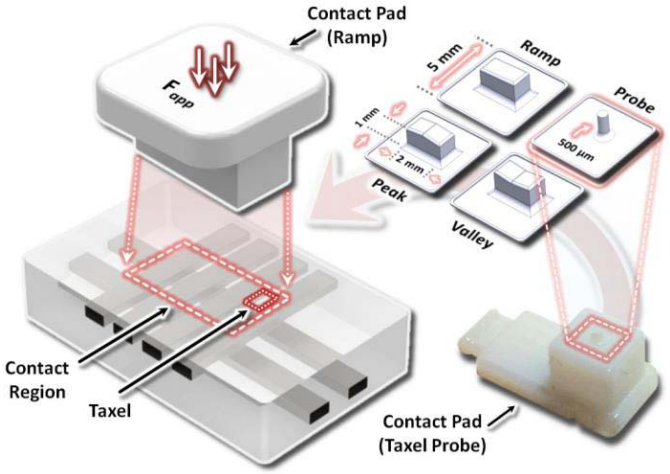

Fig. 9. Contact pads (right) include ramp, peak, and valley features which are 1mm x 2mm, and a probe feature which is 500 μm wide. The ramp, valley and peak contact pads are designed to cover all eight taxels in the sensor array when they are aligned in the sensor testbed during experiments (left).

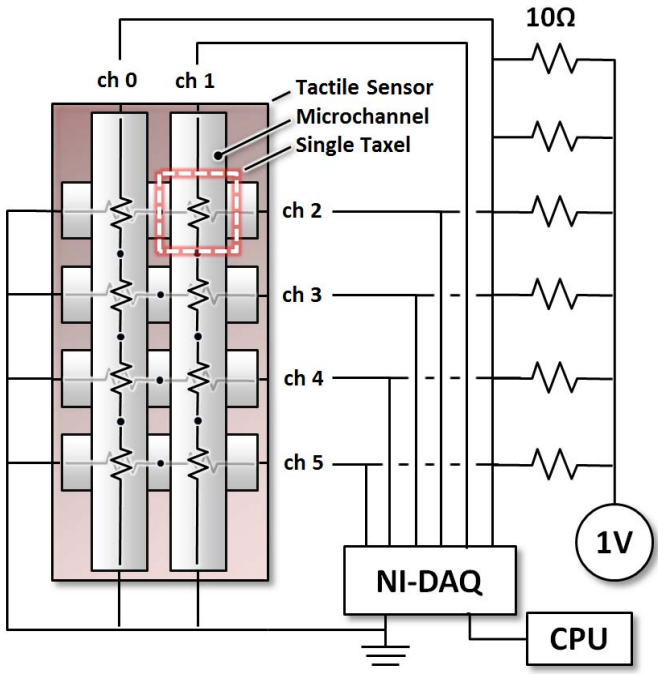

Fig. 10. An electrical schematic of the experimental setup for soft tactile sensor array mechanical testing. Resistances within the microchannels, dictated by the tactile array configuration, are shown.

- *Contact Localization:* Demonstrated by applying force over one taxel and comparing the response of the target taxel microchannels to the adjacent microchannels.
- *Determining Object Shape and Motion:* Demonstrated by visualizing microchannel output patterns for different contact pad features and contact motion (sliding).

V. Results

A. Matching Microchannel Sensitivity Ranges

The single taxel contact (Fig. 9) pad was used to characterize channel sensitivity ranges for forces up to 250mN.

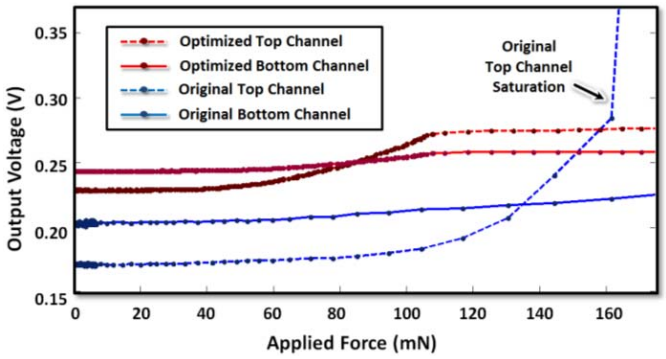

Fig. 11. The top and bottom microchannel responses at a single taxel show that neither channel saturates over the span of applied forces and that layer sensitivity ranges are more closely matched than in previous sensor [25].

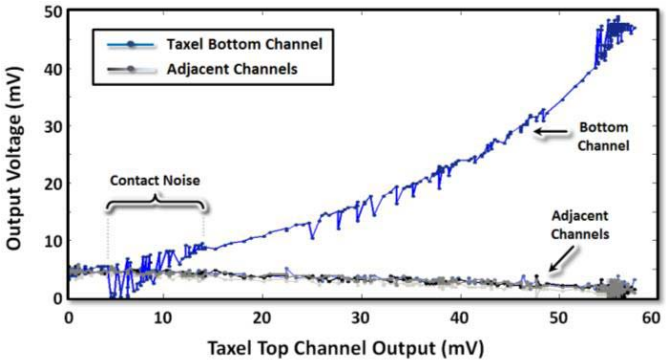

Fig. 12. Single taxel contact responses with channel voltage biases removed. Channel output voltages are plotted with respect to the top activated channel's voltage (the plot's X-axis). The increase in signal noise seen throughout manually controlled contact is likely due to hand tremor.

Experimental results show that the optimized microchannel geometries significantly improved the matching of sensitivity ranges. Fig. 11 shows that the top and bottom channels of a single sensor taxel respond to the applied forces without saturating and with similar (order of magnitude) sensitivities, unlike previous sensor [26] which experienced top channel saturation with only a marginal bottom channel response.

B. Contact Localization

The optimized soft tactile sensor, in addition to having improved sensitivity ranges, also exhibited the capacity to localize contact. Single taxel contact produced only small voltage responses in microchannels adjacent to the target taxel, an order of magnitude lower than what the target taxel microchannels exhibit. Decreases in adjacent channel voltage are likely due to cross-sectional area changes induced by target taxel microchannel deformations (Fig. 12).

Fig. 13 shows a single taxel response produced by manually controlled sensor contact. The top and bottom microchannels exhibit nearly identical output patterns, providing further evidence of channel sensitivity matching.

C. Object Shape and Motion Detection

The ability to detect the shape of objects using the tactile sensor was tested by using ramp, valley, peak-featured contact

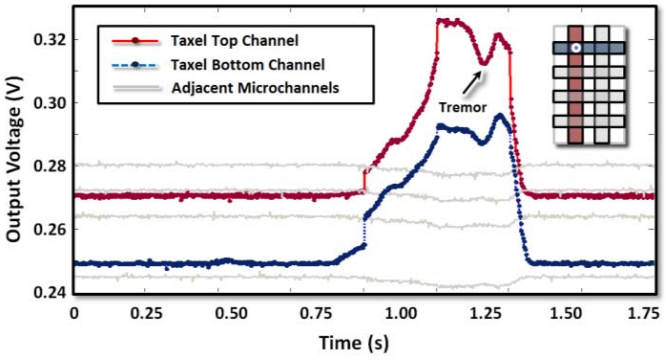

Fig. 13. Sensor response to manually controlled single-taxel contact demonstrates localization capability. Activated microchannels have strong outputs while adjacent channels exhibit much smaller responses.

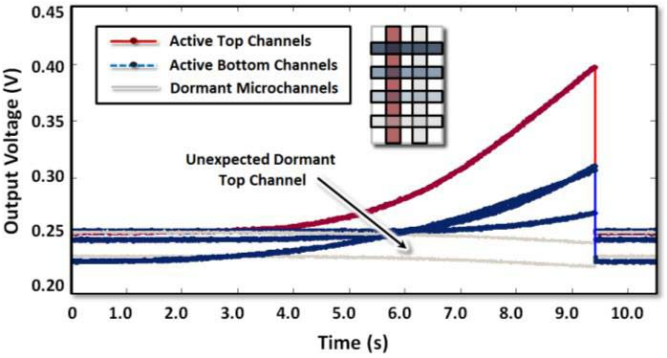

Fig. 14. Tactile sensor response to the ramp contact feature (250mN max) which activates both top microchannels and all bottom channels with descending output voltages. One top channel exhibits only a small response.

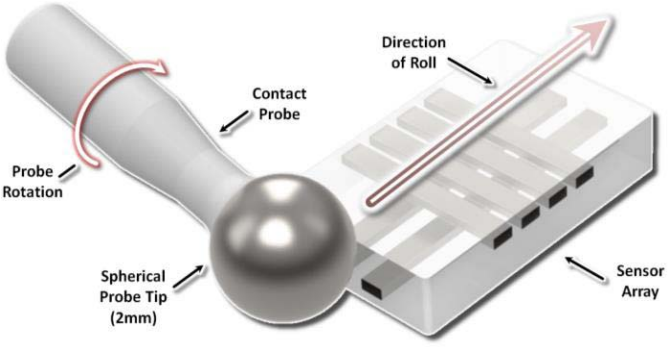

Fig. 15. Manual rolling of a spherical probe over the sensor array. Rolling was used instead of sliding to prevent shear forces at the sensor surface.

pads (Fig. 9). Results for the ramp (Fig. 14) contact pads demonstrate that the tactile sensor can discriminate abstract shapes if feature sizes are adequate (taxel-scale) and the shape is aligned on the sensors. The ramp and valley feature responses also show that the sensor can detect misalignments (misshapen contact pads due to limited rapid prototyping resolution), as seen by the dormant channels which should be active in ideal contact conditions.

The ability to detect motion across the sensor surface was tested by manually rolling a sphere-tipped mechanical probe over the microchannels (Fig. 15). The results in Fig. 16 demonstrate that the tactile sensor is able to sense contact and

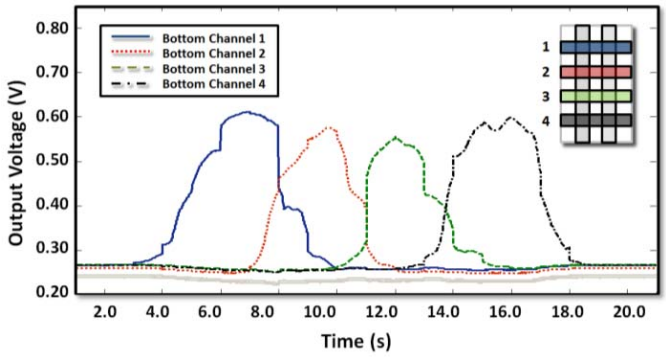

Fig. 16. Tactile sensor output voltage demonstrating the ability to detect objects (here, a spherical probe) moved manually across the sensor surface.

motion as the probe rolls at a near-constant velocity across the four bottom microchannels.

The contact sensing area of each microchannel is large enough that there is overlap between adjacent channels, enabling contact sensing at the microchannel septa. This intrinsic aliasing capability allows for motion detection as sensor-object interaction points transition from one taxel to another. This also allows localization of contact between the sensor and object features on the order of 200 microns, the sensor microchannel and septa width.

VI. Discussion

This work aimed to improve the functionality a novel soft tactile sensor array for use in micromanipulation. Our numerical optimization framework produced a sensor design solution which enables sub-millimeter contact localization and micron-level force sensing while mitigating the channel pinching and sensitivity mismatch issues encountered in the authors' previous work. Experimental results provide new insights into soft tactile sensor design and demonstrate the sensor's potential utility in micromanipulation tasks.

A. Numerically Optimizing Sensor Topology

Improvements in the performance of the sensor developed in this paper over the sensor developed in previous work emphasize the value of numerical optimization in soft sensor design. Using a robust model of the elastic mechanics of PDMS, parameterization and sensitivity analysis of the sensor design space, and formulation of a proper design quality metric, we were able to significantly improve soft tactile sensor performance without further complicating the fabrication process. The optimized microchannel geometries eliminated microchannel sensitivity mismatches and made channel pinching far less likely and severe in practice.

B. Design Guidelines

From computational and experimental data, its seems clear that the topology and, by extension, the sensitivity of the top microchannel layer governs the degree of sensitivity matching between sensor layers and that the topology of the bottom microchannel layer is likely to exhibit the same level sensitivity regardless of the top layer. We posit that thicker sensor surface layers be used to ensure that the desired range of interaction forces are transmitted more evenly to the lower microchannel layers and that upper microchannel height be tuned after specifying surface thickness to improve sensitivity matching without compromising overall performance.

C. Utility in Micromanipulation

The object shape and motion detection experiments demonstrated that the proposed tactile sensor could be used to sense the orientation of surgical needles and small mechanical components during micromanipulation, or to palpate objects to determine geometry and stiffness when vision is poor. The detection of contact pad misalignment (due to imprecisions in the rapid-prototyped parts, verified after sensor testing) suggests that this sensor may also be useful for automating grasp acquisition in robotic microassembly systems.

The sensor also demonstrated mechanical robustness, withstanding normal forces as high as 500 mN applied over one taxel – double the maximum expected total micromanipulation force. This is important for needle driving where clamping forces can reach as high as 1N.

D. Readiness for Clinical Applications

In order to be used in a clinical setting, the soft tactile sensor must be mechanically fixed to surgical instruments. The proposed sensor, due to its compliance and lack of rigid support structures, cannot easily be attached to surgical instruments as it is manufactured here. One solution to this problem is to pour the PDMS base layer of the sensor over an inextensible substrate (carbon fiber or Kevlar fabric) which can be tacked or clamped onto metallic instrument surfaces. Such fixing methods are used in several areas of soft robotics (soft actuators) and can also be applied here.

Another important aspect of the proposed sensor's clinical readiness is patient safety. Mechanical failure of the soft sensor (i.e. sensor rupturing) in a surgical setting could expose clinicians and patients to eGaIn, a bioincompatible substance. EGaIn will be replaced as the conductive medium in future sensor designs by biocompatible materials such as ionic hydrogels and conductive carbon greases.

VII. Conclusion

In this paper, a soft tactile sensor array was numerically optimized for micromanipulation. The sensor was designed to localize contact with sub-millimeter resolution, to sense forces required for microsurgical procedures, and to overcome the functional issues encountered in previous tactile sensor design work. The array was optimized by FEA to meet stringent performance requirements, fabricated using a novel, low-cost method, and empirically tested to validate the new design. The proposed sensor successfully met all performance requirements, eliminated the functional limitations of the previous design, and demonstrated force feedback capabilities essential to advanced micromanipulation tasks.

Future work will focus on larger soft tactile sensor arrays which can discriminate multiple contact locations and support aliasing for inter-taxel contact localization, the use of smaller microchannels for finer tactile resolution, and the integration of flexible circuits to enable more sophisticated wiring schemes and simplify fabrication.

ACKNOWLEDGMENT

The authors gratefully acknowledge the Wyss Institute for Biologically Inspired Engineering and the National Science Foundation for their support of this work. Any opinions, findings, and conclusions or recommendations expressed in this material are those of the authors and do not necessarily reflect the views of the National Science Foundation. The authors also thank D. Vogt for his contributions to sensor fabrication. F. L. Hammond III thanks the National Academy of Sciences for financial support through the Ford Foundation Postdoctoral Fellowship Award.

REFERENCES

[1] C. Wagner, N. Stylopoulos, and R. Howe, "The role of force feedback in surgery: Analysis of blunt dissection," in *Proc. 10th Symp. Haptic Inter. Virtual Environ. Teleoperator Syst.*, 2002, pp. 68–74.

[2] G. Tholey, J. P. Desai, and A. E. Castellanos, "Force feedback plays a significant role in minimally invasive surgery: Results and analysis," *Ann. Surgery*, vol. 241, no. 1, pp. 102–109, 2005.

[3] C.-H. King, M. O. Culjat, M. L. Franco, C. E. Lewis, E. P. Dutson, W. S. Grundfest, *et al.*, "Tactile feedback induces reduces grasping force in robot-assisted surgery," *IEEE Trans. Haptics*, vol. 2, no. 2, pp. 103–111, Apr./Jun. 2009.

[4] J. Stoll and P. DuPont, "Force control for grasping soft tissue," in *Proc. IEEE Int. Conf. Robot. Autom.*, May 2006, pp. 4309–4311.

[5] A. R. Lanfranco, A. E. Castellanos, J. P. Desai, and W. C. Meyers, "Robotic surgery—A current perspective," *Ann. Surgery*, vol. 239, no. 1, pp. 14–21, 2004.

[6] S. De, J. Rosen, A. Dagan, P. Swanson, M. Sinanan, and B. Hannaford, "Assessment of tissue damage due to mechanical stresses," in *Proc. 1st IEEE/RAS-EMBS Int. Conf. Biomed. Robot. Biomechatron.*, Feb. 2006, pp. 823–828.

[7] D. Marucci, J. Cartmill, W. Walsh, and C. Martin, "Patterns of failure at the instrument-tissue interface," *J. Surgical Res.*, vol. 93, no. 1, pp. 16–20, 2000.

[8] J. Cartmill, A. Shakeshaft, W. Walsh, and C. Martin, "High pressures are generated at the tip of Laparoscopic graspers," *Austral. New Zealand J. Surgery*, vol. 69, no. 2, pp. 127–130, 1999.

[9] A. Menciassi, A. Eisinberg, G. Scalari, C. Anticoli, M. C. Carrozza, and P. Dario, "Force feedback-based microinstrument for measuring tissue properties and pulse on microsurgery," *IEEE/ASME Trans. Mechatron.*, vol. 8, no. 1, pp. 10–17, Feb. 2003.

[10] K. Houston, C. Eder, A. Seiber, A. Menciassi, M. C. Carrozza, and P. Dario, "Polymer sensorized microgrippers using SMA actuation," in *Proc. IEEE Int. Conf. Robot. Autom.*, Apr. 2007, pp. 820–825.

[11] P. K. Gupta, P. S. Jensen, and E. deJuan, Jr., "Surgical forces and tactile perception during retinal microsurgery," in *Medical Image Computing Computer-Assisted Interventions (MICCAI)*. Cambridge, U.K.: Springer, 1999, vol. 1679, Lecture Notes in Computer Science, pp. 1218–1225.

[12] P. J. Berkelman, L. L. Whitcomb, R. H. Taylor, and P. Jensen, "A miniature microsurgcial instrument tip force sensor for enhanced force feedback during robot-assisted manipulation," *IEEE Trans. Robot. Autom.*, vol. 19, no. 5, pp. 917–921, Oct. 2003.

[13] Z. Sun, M. Balicki, K. Jin, J. Handa, R. Taylor, and I. Iordachita, "Development and preliminary data of novel optical micro-force tools for retinal surgery," in *Proc. IEEE Int. Conf. Robot. Autom.*, May 2009, pp. 1897–1902.

[14] M. A. Qasaimeh, S. Sokhanvar, J. Dargahi, and M. Kahrizi, "PVDF-based microfabricated tactile sensor for minimally invasive surgery," *J. Microelectromech. Syst.*, vol. 18, no. 1, pp. 195–207, Feb. 2009.

[15] S. Sokhanvar, M. Packirisamy, and J. Dargahi, "A multifunctional PVDF-based tactile sensor for minimally invasive surgery," *Smart Mater. Struct.*, vol. 16, pp. 989–998, Aug. 2007.

[16] B. L. Gray and R. S. Fearing, "A surface micromachined microtactile sensor array," in *Proc. IEEE Int. Conf. Robot. Autom.*, Apr. 1996, pp. 1–6.

[17] K. Kim, X. Liu, Y. Zhang, and Y. Sun, "MicroNewton force-controlled manipulation of biomaterials using a monolithic MEMS microgripper with two-axis force feedback," in *Proc. IEEE ICRA*, May 2008, pp. 3100–3105.

[18] H. Chu, J. Mills, and W. Cleghorn, "MEMS capacitive force sensor for use in microassembly," in *Proc. IEEE/ASME Int. Conf. Adv. Intell. Mechatron.*, Jul. 2008, pp. 797–802.

[19] Y. Sun, W. Choi, H. Jiang, Y. Huang, and J. Rogers, "Controlled buckling of semiconductor nanoribbons for stretchable electronics," *Nature Nanotechnol.*, vol. 1, no. 3, pp. 201–207, 2006.

[20] S. P. Lacour, S. Wagner, H. Zhenyu, and Z. Suo, "Stretchable gold conductors on elastomeric substrates," *Appl. Phys. Lett.*, vol. 82, no. 15, pp. 2404–2406, 2003.

[21] D. Cotton, I. M. Graz, and S. P. Lacour, "A multifunctional capacitive sensor for stretchable electronic skins," *IEEE Sensors J.*, vol. 9, no. 12, pp. 2008–2009, Dec. 2009.

[22] Y. L. Park, C. Majidi, R. Kramer, P. Berard, and R. J. Wood, "Hyperelastic pressure sensing with a liquid-embedded elastomer," *J. Micromech. Microeng.*, vol. 20, no. 12, p. 125029, 2010.

[23] H. B. Muhammad, C. M. Oddo, L. Beccai, C. Recchiuto, C. J. Anthony, M. J. Adams, *et al.*, "Development of a ioinspired MEMS based capacitive tactile sensor for a robotic finger," *Sens. Actuators A, Phys.*, vol. 165, no. 2 pp. 221–229, 2011.

[24] D. Marucci, J. Cartmill, C. Martin, and W. Walsh, "A compliant tip reduces the peak pressure laparoscopic graspers," *ANZ J. Surgery*, vol. 72, no. 7, pp. 476–478, 2002.

[25] P. Peng and R. Rajamani, "Flexible microtactile sensor for normal and shear elasticity measurements," *IEEE Trans. Ind. Electron.*, vol. 59, no. 12, pp. 4907–4913, Dec. 2012.

[26] F. L. Hammond, R. K. Kramer, R. D. Howe, and R. J. Wood, "Soft tactile sensor arrays for micromanipulation," in *Proc. IEEE Int. Conf. Robot. Intell. Syst.*, Oct. 2012, pp. 25–32.

[27] R. Kramer, C. Majidi, and R. J. Wood, "Wearable tactile keypad with stretchable artificial skin," in *Proc. IEEE Int. Conf. Robot. Autom.*, May 2011, pp. 1103–1107.

[28] Y. L. Park, B. Chen, and R. J. Wood, "Design and fabrication of soft artifical skin using embedded microchannels and liquid conductors," *IEEE Sensors J.*, vol. 12, no. 8, pp. 2711–2718, Aug. 2011.

[29] D.-S. Kwon, K. Y. Woo, S. K. Song, W. S. Kim, and H. S. Cho, "Microsurgical telerobot system," in *Proc. IEEE/RSJ Int. Conf. Intell. Robot. Syst.*, Oct. 1998, pp. 945–950.

[30] J. Zang, X. Zhao, Y. Cao, and J. W. Hutchinson, "Localized ridge wrinkling of stiff films on compliant substrates," *J. Mech. Phys. Solids*, vol. 60, no. 7, pp. 1265–1279, 2012.

[31] S.-H. Yoon, V. Reyes-Oritz, K.-H. Kim, Y. Ho Seo, and M. R. K. Mofrad, "Analysis of circular PDMS microballons with ultralarge deflection for MEMS design," *J. MEMS Syst.*, vol. 19, no. 4, pp. 854–864, 2010.

[32] M. D. Dickey et. al, "Eutectic gallium-indium (EGaIn): A liquid metal alloy for the formation of stable structures in microchannels at room temperature," *Adv. Funct. Mat.*, vol. 18, no. 7, pp. 1097–1104, 2008.

[33] F. Hammond, S. Talbot, R. Howe, and R. Wood, "Measurement system for the characterization of micromanipulation motion and force," in *Proc. Des. Med. Devices Conf.*, 2013, pp. 1–2.

Frank L. Hammond III (M'08) received the B.S. degree in electrical engineering from Drexel University in 2002, the M.S. degree in electrical and mechanical engineering from the University of Pennsylvania in 2006, and the Ph.D. degree in mechanical engineering from Carnegie Mellon University in 2010, where his thesis focused on contextual design optimization of kinematically redundant manipulators. He is currently a Post-Doctoral Research Fellow with the Harvard School of Engineering and Applied Sciences and the Wyss Institute for Biologically Inspired Engineering, where his research focuses on dexterous robotic manipulation and the design of underactuated robotic hands.

Rebecca K. Kramer is an Assistant Professor of mechanical engineering with Purdue University. Her research interests include soft active materials, microfabrication of smart surfaces, and stretchable sensors and electronics. She received the Ph.D. degree in engineering sciences from Harvard University, the M.S. degree in mechanical engineering from the University of California at Berkeley, and the B.S. degree in mechanical engineering from Johns Hopkins University.

Qian Wan is a graduate student at the Harvard School of Engineering and Applied Sciences. She received the B.Sc. degree in engineering from Princeton University and was a Research Assistant with the McGovern Institute for Brain Research, Massachusetts Institute of Technology. Her current research interests include underactuated robotic hands.

Robert D. Howe (F'12) is the Abbott and James Lawrence Professor of engineering, Director of undergraduate studies for biomedical engineering, and Area Dean of bioengineering with the Harvard School of Engineering and Applied Sciences. He received the bachelor's degree in physics from the Reed College. He then worked in the electronics industry in Silicon Valley. He received the Doctoral degree in mechanical engineering from Stanford University. He then joined the faculty at Harvard in 1990. He directs the Harvard BioRobotics Laboratory, which investigates the roles of sensing and mechanical design in motor control, in both humans and robots. His research interests focus on manipulation, the sense of touch, haptic interfaces, and robot-assisted and image-guided surgery.

Robert J. Wood (M'01) received the M.S. and Ph.D. degrees from the Department of Electrical Engineering and Computer Sciences, University of California, Berkeley, in 2001 and 2004, respectively. He is currently the Charles River Professor of engineering and applied sciences with the Harvard School of Engineering and Applied Sciences, and is a Founding Core Faculty Member of the Wyss Institute for Biologically Inspired Engineering, Harvard University, Boston, MA, USA. His current research interests include microrobotics and bioinspired robotics.